Catal Lett (2009) 129:93–103
DOI 10.1007/s10562-008-9838-1

Application of the Selective Energy Transfer Model to Account for an Isokinetic Response in the Gas Phase Reductive Cleavage of Hydroxyl, Carbonyl and Carboxyl Groups from Benzene Over Nickel/Silica

Mark A. Keane · Ragnar Larsson

Received: 21 November 2008 / Accepted: 25 December 2008 / Published online: 17 January 2009

Abstract The gas phase hydrodeoxygenation of a series of aromatic alcohols, aldehydes and acids has been examined over Ni/SiO_2. Compensation behaviour is established with an isokinetic temperature (518 ± 21 K) that is consistent with with the point of intersection of the Arrhenius lines. This is accounted for using the Selective Energy Transfer model that is based on resonance between the catalytic Ni–H vibration and out-of plane C–H vibrations of the aromatic reactants with a transferral of resonance energy from the catalyst to generate the "activated complex". The calculated wave number of this vibration mode is $720 \pm 29\ cm^{-1}$ with an associated anhamonicity of $-3.3 \pm 0.9\ cm^{-1}$. Our analysis suggests that the oxygenated aromatic is weakly adsorbed on the catalyst and surface mobility facilitates reaction with adsorbed hydrogen atoms.

Keywords Isokinetic temperature · Selective energy transfer model · Anharmonicity · Catalytic hydrodeoxygenation · Ni/silica

1 Introduction

In a series of earlier studies [1–3], we examined the isokinetic effect for the reductive cleavage of C–X bonds in a range of haloarenes over supported Ni catalysts. An isokinetic response occurs where the Arrhenius plots (ln k vs. $1/T$) for a series of related reactions intersect at a common temperature (the isokinetic temperature, T_{iso}). We demonstrated that the T_{iso} for hydrodehalogenation could be accounted for using the Selective energy transfer (SET) model [1]. The basis for the SET model is the occurrence of a state of resonance between a vibrational mode of the catalyst system and a complementary vibrational mode of the reacting molecule. We identified the critical reactant vibrational mode as an out-of-plane C–H vibration with optimum resonance energy transfer from the catalyst (Ni–H) vibrational mode [1, 3]. We have now extended that work and report here an SET analysis of the hydrogenolytic cleavage of oxygenated functional groups from the aromatic ring.

Light petroleum feedstocks are increasingly being replaced by heavy oils, shale or coal oils and these heavy fossil fuels must be pretreated to prevent poisoning of the cracking catalysts by sulphur, nitrogen and oxygen containing compounds [4]. Catalytic hydrodeoxygenation has assumed increasing importance in the upgrading of coal-derived and biomass-derived liquids and in the conversion of waste plastics to hydrocarbon raw material or fuel [5–7]. Substituted benzene systems have been used to evaluate the hydrogenolysis versus ring hydrogenation activity of typical hydrotreating catalysts [8, 9]. Hydrogenolysis reactions require a site ensemble of two or more metal atoms [10] where little or no hydrogenolytic activity is exhibited by homogeneous catalysts [11]. Ring hydrogenation occurs in preference to hydrogenolysis over Ru and Rh systems while Ni catalysts are known to exhibit appreciable hydrogenolytic behaviour [11, 12]. Conventional hydro processing catalysts, such as $CoMo/Al_2O_3$ and $NiMo/Al_2O_3$ have been widely used in hydrodeoxygenation

M. A. Keane (✉)
Chemical Engineering, School of Engineering and Physical Sciences, Heriot-Watt University, Edinburgh EH14 4AS, Scotland
e-mail: M.A.Keane@hw.ac.uk

R. Larsson
Chemical Engineering II, University of Lund, P.O. Box 124, 221 00 Lund, Sweden

applications [5, 13–15]. These catalysts are much more active in their sulphided form but the oxygen content of the feed can have a deleterious effect on the sulphide structure resulting in losses in activity and changes in product distribution [16]. Although the gas phase Ni catalysed hydrogenolysis of simple hydrocarbons is well established, the authors could find no detailed kinetic studies of the hydrogenolysis of oxygen bearing aromatics (hydrodeoxygenation). Kinetic data for the gas phase hydrogen mediated cleavage of $–CH_2OH$, –CHO and –COOH substituents from benzene (and toluene) in the presence of Ni/SiO_2 are presented in this paper. We have undertaken a rigorous analysis of the significance of the experimentally determined isokinetic temperature in catalytic hydrodeoxygenation.

2 Experimental Procedure

2.1 Catalyst Preparation, Activation and Characterisation

The catalyst was prepared by the homogeneous precipitation/deposition of nickel onto Cab-O-Sil 5 M silica (surface area 194 $m^2\ g^{-1}$), which had been washed with triply deionized water and dried in air for 20 h at 383 K before use. The precipitation was carried out in a 2 dm^3 three-necked round-bottomed flask fitted with a Citenco motor driven stirrer. A sample of urea (Aldrich Chem. Co., 99+%) was added to a 1.5 dm^3 aqueous suspension of Cab-O-Sil 5 M in nickel nitrate (Aldrich Chem. Co., 99.999%) at 290 ± 2 K, where the molar ratio of the nitrate to urea was 0.36 and the suspension was slowly heated under constant agitation (600 rpm) to 361 ± 3 K and held at this temperature for 6 h. The pH of the suspension was pre-adjusted (with HNO_3) to 2.8 to prevent premature hydrolysis and the pH was observed to increase to 5.3 on completion of the precipitation step. The suspension was then filtered and the filtrate washed with 4 × 400 cm^3 hot deionized water and air-dried in an oven at 383 K for 20 h. The Ni loading (1.5 % w/w) was determined (to within ±2%) by inductively coupled plasma-optical emission spectrometry (ICP-OES, Vista-PRO, Varian Inc.) from the diluted extract of aqua regia; water content of the dried catalyst precursor (Pye Unicam thermobalance) <1% w/w. Prior to catalysis, the catalyst precursor, sieved in the 75–150 μm mesh range, was reduced by heating in a 150 $cm^3\ min^{-1}$ stream of hydrogen at a fixed rate of 5 K min^{-1} (controlled using a Barber–Coleman temperature programmer) to a final temperature of 773 ± 1 K which was maintained for 18 h. The hydrogen gas (99.9%) was purified by passage through water (activated Molecular Sieve type 5A) and oxygen (1% Pd on WO_3) traps, which were connected in series. A full temperature programmed reduction analysis has been reported previously [17]. BET surface area and H_2 uptake measurements (reproducible to within ±5%) were conducted using the commercial CHEMBET 3000 unit (Quantachrome Instruments); the procedure is described in detail elsewhere [18, 19]. Nickel particle size was determined by transmission electron microscopy: JEOL 2000 TEM microscope operated at an accelerating voltage of 200 kV. The catalyst samples were dispersed in 1-butanol by ultrasonic vibration, deposited on a lacey-carbon/Cu grid (300 mesh) and dried at 383 K for 12 h. The surface area weighted mean diameter quoted in this paper is based on a count of 685 individual Ni particles.

2.2 Catalysis Procedure

The catalytic reactions were carried out under atmospheric pressure in a fixed bed glass reactor (i.d. = 15 mm) in the overall temperature range $403 \leq T \leq 603$ K. The catalyst was supported on a glass frit and a layer of glass beads above the catalyst bed ensured that the aromatic reactant reached the reaction temperature before contacting the catalyst. Isothermal operation was maintained by diluting the catalyst bed with ground glass (75–150 μm). Interparticle and intraparticle heat transport effects can be disregarded when applying established criteria [20]; the temperature differential between the catalyst particle and bulk fluid phase was <1 K. Plug-flow conditions applied with reactor diameter/catalyst particle ratio of 133. Full details of the catalytic reactor/procedure including the approach taken to assess mass transport contributions under reaction conditions are available elsewhere [21]. The catalytic system was found to operate with negligible diffusion retardation of the reaction rate; effectiveness factor (η) > 0.99. A Sage pump (model 341 B) was carefully calibrated and used to deliver the aromatic feed via a glass/PTFE air-tight syringe and PTFE line at a fixed rate. The aromatic vapour was carried through the catalyst bed in a stream of purified H_2, the flow rate of which was set using Brooks mass flow controllers. The kinetic measurements were made over a catalyst weight (W) to inlet molar aromatic flow rate (F) ratio in the range 5–180 g h mol where the H_2 partial pressure was in the range 0.91–0.99 atm and H_2 was at least 15 times in excess relative to stoichiometric quantities. The reactor effluent was either sampled on-line via a 20 × 10^{-6} dm^3 sampling valve or was frozen in a liquid nitrogen trap for subsequent off-line analysis. Product analysis was made using a Varian 3400 GC chromatograph equipped with a flame ionization detector and employing a 30% Silicone SF96 on 60/80 mesh acid washed Chromosorb W (6 ft × 1/8 in.) stainless steel column; the detection limit corresponded to a

feedstock conversion <0.1 mol%. The overall level of hydrodeoxygenation was converted to mol% conversion using detailed (at least 20 point) calibration plots for each of the aromatic reactants. Each reactant (Aldrich, >98%) was thoroughly degassed by purging with purified helium followed by a series of freeze/pump/thaw cycles and were stored over activated molecular sieve type 5A. The experimentally determined rate constants are given in Table 1, wherein the range of aromatic feedstock that was studied is identified. In a series of blank tests, passage of each reactant in a stream of H_2 through the empty reactor, i.e. in the absence of catalyst, did not result in any detectable conversion. All the data presented here have been generated in the absence of any significant catalyst deactivation where each catalytic run was repeated (up to six times) using different samples from the same batch of catalyst: the measured rates did not deviate by more than ±6%.

3 Results and Discussion

3.1 Catalyst Characteristics

The Ni loading, BET surface area and Ni dispersion/particle diameter/surface area obtained from H_2 chemisorption and HRTEM measurements, are given in Table 2. The agreement in terms of the average Ni particle diameter obtained from both analytical techniques is reasonable. The representative TEM image provided in Fig. 1 serves to illustrate the nature of the metal dispersion where the Ni particles exhibit a pseudo–spherical morphology and a narrow (<1–5 nm) size distribution. Ni/SiO_2 preparation by deposition–precipitation has been shown elsewhere [17, 22, 23] to generate smaller average Ni particle diameters when compared with the less controlled impregnation route. It has been established [24] that deposition–precipitation results in the formation of a nickel phyllosilicate phase, which is responsible for enhanced Ni dispersion [24].

3.2 Catalytic Data Analysis

The raw kinetic data given in Table 1 are presented in Fig. 2 as conventional Constable plots [25, 26], i.e. ln A (the experimentally determined Arrhenius pre-exponential factor) versus E_a (the experimental activation energy). The linear plots are characteristic of what has become known as a compensation effect. The use of the "compensation" descriptor is an attempt to reconcile the seemingly paradoxical situation where an increase in activation energy is accompanied by an increase in the pre-exponential factor [25]. The experimental rate constants (and associated

Table 1 Collation of the experimental hydrodeoxygenation kinetic data

Reactant	$10^3/T$ (K^{-1})	ln (kmol h^{-1} g^{-1})	E_a (kJ mol^{-1})	ln A
Benzyl alcohol	2.481	−12.62	52.2	2.94
	2.421	−12.25		
	2.364	−11.90		
	2.309	−11.56		
	2.257	−11.13		
	2.183	−10.79		
	2.114	−10.32		
	2.008	−9.87		
	1.949	−9.40		
	1.894	−9.01		
	1.876	−8.68		
	1.842	−8.49		
m-methyl benzyl alcohol	2.421	−12.45	46.4	1.17
	2.364	−12.11		
	2.336	−11.91		
	2.283	−11.58		
	2.232	−11.20		
	2.137	−10.66		
	2.092	−10.38		
	2.028	−10.03		
	1.969	−9.75		
	1.912	−9.47		
	1.876	−9.33		
	1.842	−9.20		
	1.808	−9.10		
Benzaldehyde	2.257	−12.68	86.6	10.91
	2.232	−12.50		
	2.208	−12.26		
	2.183	−11.84		
	2.160	−11.54		
	2.114	−10.95		
	2.049	−10.26		
	2.028	−10.14		
	2.008	−9.88		
	1.949	−9.41		
	1.931	−9.32		
	1.894	−9.01		
	1.842	−8.33		
	1.808	−7.94		
	1.776	−7.62		
m-tolualdehyde	2.208	−12.02	70.3	6.74
	2.160	−11.60		
	2.137	−11.33		
	2.114	−11.08		
	2.070	−10.69		
	2.003	−10.32		
	1.988	−9.99		

Table 1 continued

Reactant	$10^3/T$ (K^{-1})	ln (kmol h^{-1} g^{-1})	E_a (kJ mol^{-1})	ln A
	1.949	−9.76		
	1.912	−9.44		
	1.876	−9.19		
	1.842	−9.02		
	1.808	−8.71		
	1.792	−8.32		
	1.745	−7.90		
Benzoic acid	2.028	−12.46	74.7	5.90
	1.988	−12.03		
	1.949	−11.58		
	1.912	−11.32		
	1.876	−10.88		
	1.842	−10.54		
	1.808	−10.23		
	1.776	−9.96		
	1.745	−9.78		
	1.715	−9.57		
	1.686	9.34		
	1.658	9.11		
m-toluic acid	1.988	−12.11	66.9	3.80
	1.949	−11.80		
	1.912	−11.56		
	1.876	−11.30		
	1.859	−11.16		
	1.842	−11.02		
	1.808	−10.83		
	1.792	−10.64		
	1.776	−10.56		
	1.761	−10.49		
	1.745	−10.28		
	1.730	−10.07		
	1.715	−9.93		
	1.686	−9.67		
	1.658	−9.43		
o-terephthaldehyde	2.283	−11.51	55.4	3.84
	2.257	−11.19		
	2.207	−10.88		
	2.160	−10.56		
	2.114	−10.21		
	2.070	−9.92		
	2.049	−9.72		
	2.008	−9.45		
	1.969	−9.26		
	1.931	−9.04		
	1.912	−8.92		
	1.859	−8.64		
	1.808	−8.25		
	1.776	−8.00		

Table 1 continued

Reactant	$10^3/T$ (K^{-1})	ln (kmol h^{-1} g^{-1})	E_a (kJ mol^{-1})	ln A
o-phthalic acid	1.949	−12.84	113.3	13.74
	1.912	−12.46		
	1.876	−11.81		
	1.859	−11.57		
	1.842	−11.33		
	1.808	−10.78		
	1.792	−10.56		
	1.776	−10.38		
	1.761	−10.16		
	1.745	−9.96		
	1.715	−9.76		
	1.701	−9.57		
	1.686	−9.21		
	1.658	−8.88		

Table 2 Ni content, BET surface area and metal phase characteristics associated with the activated Ni/SiO_2 catalyst

% Ni w/w	1.5
BET surface area (m^2 g^{-1})	183
Ni particle size (nm)	1.4[a], 2.2[b]
Ni particle size range (nm)	<1–5[a]
Ni dispersion (%)	47[a]
Ni surface Area (m^2 g_{Ni}^{-1})	310[a]

[a] From TEM analysis

[b] From H_2 chemisorption analysis

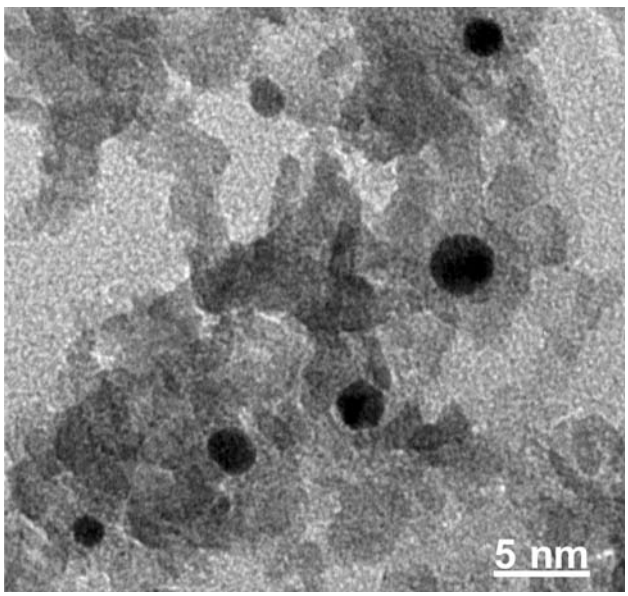

Fig. 1 Representative TEM image of Ni/SiO_2

activation energies) refer solely to the catalytic hydrogenolytic cleavage of the alcohol, acid or aldehyde groups to deliver the parent aromatic (benzene or toluene). A preliminary plot of the experimental kinetic results has revealed that the data for the aromatic acid reactants (benzoic acid, *m*-toluic acid and *o*-phthalic acid) do not fall on the same line as the alcohol/aldehyde reactants (benzyl alcohol, *m*-methyl benzyl alcohol, benzaldehyde, *m*-tolualdehyde and *o*-terephthaldehyde). An important feature of our analysis of the kinetic data is the identification of an isokinetic point, i.e. the Arrhenius lines (ln k vs. $1/T$) intersect at a common (isokinetic) point. The abscissa value associated with that point defines the isokinetic temperature (T_{iso}). As a first approximation the data associated with the aromatic alcohols and aldehydes were used (in Fig. 2) to define a line from which the slope ($b = 0.2{,}340$ mol kJ^{-1}) can be used to calculate T_{iso} according to [25]

$$T_{iso} = 1/(R \times b) \quad (1)$$

with an associated $T_{iso} = 514$ K. A second (dashed) line has been included in Fig. 2, parallel to the Constable plot for the alcohols/aldehydes and positioned to coincide with the experimental points for the aromatic acids. It can be seen that the entries for benzoic and *m*-toluic acid fall on this line and, within reasonable error limits, these reactants can be included in a group of reactants with $T_{iso} = 514$ K. However, the datum point for *o*-phtalic acid does not adhere to this treatment and can not be readily included in the Constable plot. The range of reactivities associated with the reactants considered in this study can be assessed

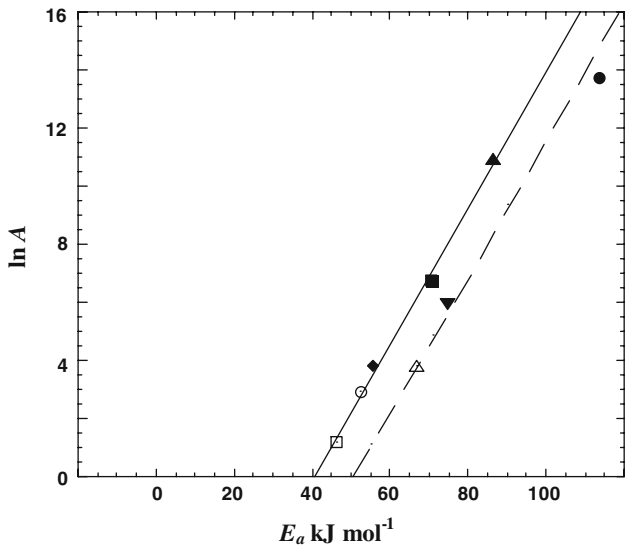

Fig. 2 Constable plots associated with the hydrodeoxygenation of benzyl alcohol (○), *m*-methyl benzyl alcohol (□), benzaldehyde (▲), m-tolualdehyde (■), benzoic acid (▼), *m*-toluic acid (Δ), *o*-terephthaldehyde (◆) and *o*-phthalic acid (●): see Table 1

Table 3 Specific hydrodeoxygnation rate constants (k') at a representative reaction temperature (523 K)

Reactant	$10^2\ k'$ [mol h^{-1} (m^2 g_{Ni}^{-1})$^{-1}$]
Benzyl alcohol	206
m-methyl benzyl alcohol	155
Benzaldehyde	214
m-tolualdehyde	159
Benzoic acid	24
m-toluic acid	19
o-terephthaldehyde	266
o-phthalic acid	8

from the specific rates given in Table 3 for a representative reaction temperature. The T_{iso} extracted from this analysis is of practical value as it may represent a suitable working temperature at which to conduct the hydrodeoxygenation of a mixed aromatic feed.

In terms of the SET treatment [27, 28], the simplest possible relationship takes the form

$$T_{iso} = Nhc/2Rv = 0.719v \quad (2)$$

where v is the vibrational frequency (wave number) of the reactant that, in resonance with a vibrational mode of the catalyst, "distorts" the reactant molecule to arrive at the structure in the activated state, which is necessary for catalytic conversion. It should be noted that the wave number of this critical vibration mode ($514/0.719 = 715$ cm^{-1}) as derived from Eq. 2 only applies to a "perfect" resonance, i.e. the frequency of the reactant molecule (v) is the same as that of the catalyst system (ω), from which there is a transferral of resonance energy. As the catalyst system in effect donates energy, the expression "heat bath" has been applied to the donating system. In Fig. 3 we have applied the rule of Linert [26] that the isokinetic temperature should be derived from the intersection point of the Arrhenius lines. A visual inspection of the Arrhenius plots for the alcohol and aldehyde reactants suggests a common point of intersection at $1{,}000/T =$ ca. 2 K^{-1}. However, the crossing point is not clearly defined in Fig. 3 and so, to improve clarity, we have divided the Arrhenius plots into three groups, presented in Fig. 4a–c. The lines for *m*-methyl benzyl alcohol and *m*-tolualdehyde (Fig. 4a) intersect at ln $k = -9.59$ mol h^{-1} g^{-1} and $1{,}000/T = 1.93$ K^{-1}; the value of the abscissa corresponds to $T_{iso} = 518$ K. In the case of the two groups presented in Fig 4b, c, there are three crossing points for each group, which are presented in Table 4. The mean value of the seven entries results in $T_{iso} = 518 \pm 21$ K, which according to Eq. 2 corresponds to $v = 720 \pm 29$ cm^{-1}. This value is in reasonable agreement with that derived from the slope of the Constable plot (715 cm^{-1}). It should be noted that the k_{iso} associated with the aromatic acids is

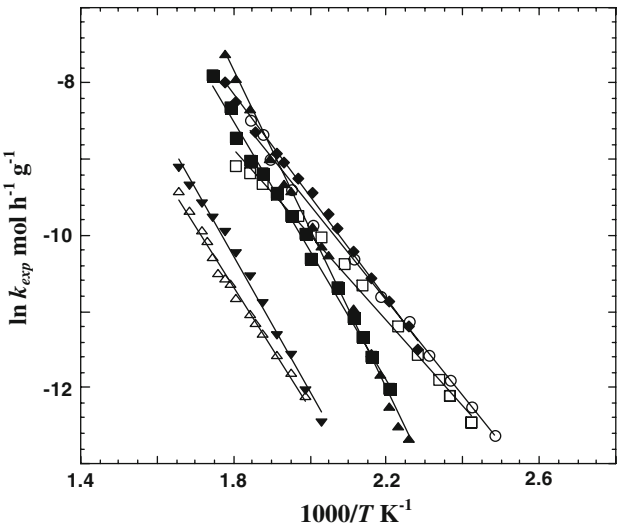

Fig. 3 Arrhenius plots for the hydrodeoxygenation of benzyl alcohol (○, correlation coefficient = 0.9975), *m*-methyl benzyl alcohol (□, correlation coefficient = 0.9971), benzaldehyde (▲, correlation coefficient = 0.9975), *m*-tolualdehyde (■, correlation coefficient = 0.9970), benzoic acid (▼, correlation coefficient = 0.9966), *m*-toluic acid (Δ, correlation coefficient = 0.9960) and *o*-terephthaldehyde (◆, correlation coefficent = 0.9984)

appreciably lower. It has, however, been demonstrated [2, 29] that related systems with a common T_{iso} (common intersection at the abscissa) can exhibit a significant difference in the ordinate position, indicating differences in "collision number", i.e. that component of the rate constant which is not dependent on the vibrational resonance effects [27]. The analysis thus far has established that the hydrodeoxygenation of eight aromatic alcohols, aldehydes and acids over Ni/SiO_2 share a common isokinetic temperature and, as a direct consequence, the same wave number for the critical vibration mode, i.e. 720 ± 29 cm^{-1}.

3.3 Activation Energies

The activation energies were all determined by a standard Arrhenius treatment of the experimentally determined kinetic data given in Table 1. While *o*-phthalic acid deviated from the other seven reactants in terms of the Constable plot, it could be accommodated in one of the groups presented in Table 4 and we have included this dataset in the following treatment of hydrodeoxygenation activation energies. In an earlier application of the SET model [3], we established a stepwise variation in the experimental activation energy with one common least term. In the SET treatment, the activation energy is considered to be the sum of a series of vibrational quanta. The vibrational modes in a molecule are anharmonic, resulting in an unequal spacing of the energy levels. For systems where the anharmonicity

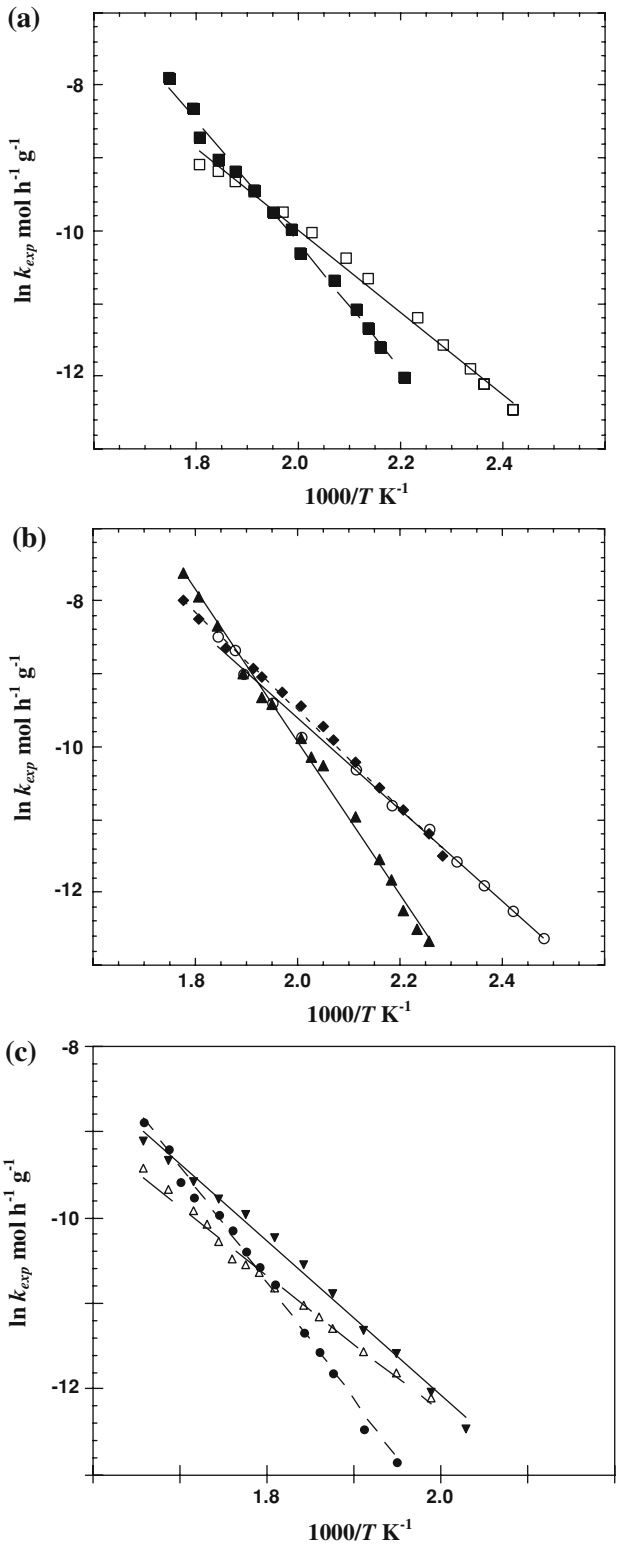

Fig. 4 Arrhenius plots for the hydrodeoxygenation of: **a** *m*-methyl benzyl alcohol (□) and *m*-tolualdehyde (■); **b** benzyl alcohol (○), benzaldehyde (▲) and *o*-terephthaldehyde (◆); **c** benzoic acid (▼), *m*-toluic acid (Δ) and *o*-phthalic acid (●, correlation coefficient = 0.9971)

Table 4 Calculation of T_{iso} from the Arrhenius plots presented in Fig. 4, according to approach recommended by Linert [26]

Reactant	Equation of the linear curve fitting	Point of intersection			T_{iso} (K)
			ln k_{iso}	1,000/T_{iso}	
m-tolualdehyde (1)	$y = 6.7695 - 8.4822x$	(1)/(2)	−9.59	1.93	518.4
m-methyl benzyl alcohol (2)	$y = 1.3178 - 5.6563x$				
Benzyl alcohol (3)	$y = 2.9465 - 6.2799x$	(3)/(4)	−9.12	1.92	520.6
Benzaldehyde (4)	$y = 10.904 - 10.422x$	(4)/(5)	−8.69	1.88	531.9
o-terephtaldehyde (5)	$y = 3.8533 - 6.6717x$	(3)/(5)	−11.62	2.32	431.2
Benzoic acid (6)	$y = 5.8884 - 8.9827x$	(6)/(7)	−14.00	2.21	451.7
m-toluic acid (7)	$y = 3.7995 - 8.0393x$	(6)/(8)	−9.31	1.69	591.0
o-phtalic acid (8)	$y = 13.735 - 13.619x$	(6)/(7)	−10.2	1.78	561.5
$T_{iso} \pm$ RMS (K)					518 ± 21
$v \pm$ RMS (cm^{-1})					720 ± 29

constant is small, the difference between two values of activation energies should be a sum of vibrational quanta. Following the approach we have set out previously [2], we first estimate the least common term describing the differences in the series of experimental activation energies (E_a), including a correction for RT_{mean} where T_{mean} represents the mean temperature for each dataset. The consecutive differences between the $E_a - RT_{mean}$ values are given in Table 5 where this series can be expressed as a multiple of a least common term [30]. From a consideration of lower value terms [$\Delta(E_a - RT_{mean}) < 20$ kJ mol^{-1}] we have chosen eight as a first approximation, divided each entry in the series by this estimated value and taken the resulting figure to the nearest whole number (which we denote n'). A more precise value of the common least term (E_0) can be obtained from [3]

$$E_0 = \sum \Delta(E_a - RT_{mean}) / \sum n' \tag{3}$$

and equals 8.1 kJ mol^{-1}. The parameter E_0 is related to (but is not identical to) the critical reactant vibrational frequency (v) that results in conversion. Ideally, this freqency should be the same as that derived from the slope of the Constable plot [27]. The activation energy corresponds to the sum of the vibrational quanta of the specific vibration mode in the reacting molecule that deforms the molecule towards the structure of the "activated state" [27], where

$$E_a - RT + Q = nv_0 + v_0 x_0 n^2 \tag{4}$$

This equation follows from spectroscopic theory where the vibrational energy [$G_0(n)$] of a particular vibrational mode is given by [30]

$$G_0(n) = nv_0 + v_0 x_0 n^2. \tag{5}$$

The parameter x_0 is the anharmonicity constant and we identify the enthalpy of activation ($E_a - RT$) with the vibrational energy above zero state; Q is a term representing the heat of adsorption. We are now in a position to develop an analytical expression for E_0. Taking two vibrational quantum numbers n_i and n_j, we can express $\Delta(E_a - RT)$ by

$$\begin{aligned} \Delta(E_a - RT)_{i,j} &= (n_i - n_j)v_0 + v_0 x_0 \left(n_i^2 - n_j^2\right) \\ &= (n_i - n_j)\left[v_0 + v_0 x_0 (n_i + n_j)\right] \end{aligned} \tag{6}$$

Similarly, for vibrational quantum numbers n_j, n_k and n_k, n_l, the analogous expressions apply

Table 5 Analysis of consecutive differences of the experimentally determined activation energies

E_a (kJ mol^{-1})	T_{mean} (K)	$E_a - RT_{mean}$ (kJ mol^{-1})	$\Delta(E_a - RT_{mean})$ (kJ mol^{-1})	n'	$(E_a - RT_{mean})/E_0$	n	$n_i + n_j$
52.2	473	48.27	5.89	1	5.96	6	11
46.4	483	42.38	40.04	5	5.23	5	15
86.6	503	82.42	16.38	2	10.18	10	18
70.3	513	66.04	4.1	0	8.15	8	17
74.7	548	70.14	7.84	1	8.66	9	17
66.9	553	62.30	11.07	1	7.69	8	14
55.4	501	51.23	57.47	7	6.32	6	19
113.3	558	108.70	60.43	8	13.42	13	19

$$\Delta(E_a - RT)_{j,k} = (n_j - n_k)\left[v_0 + v_0 x_0 (n_j + n_k)\right] \quad (7)$$

$$\Delta(E_a - RT)_{k,l} = (n_k - n_l)[v_0 + v_0 x_0 (n_k + n_l)] \quad (8)$$

It should be noted that the differences $(n_i - n_j)$ etc. correspond to the term n' given above. Approximate values of the vibrational quantum number can be arrived at by setting n equal to the integer value of $(E_a - RT)/E_0$, neglecting the Q and anharmonic terms in Eq. 4; values of n to the nearest whole number are given in Table 5. The sum $(n_i + n_j)$, while not constant, does not vary greatly. Denoting the mean of the values by $n_x + n_y$ (=16)

$$\sum \Delta(E_a - RT) = \sum n'\left[v_0 + v_0 x_0 (n_x + n_y)\right] \quad (9)$$

$$E_0 = \sum \Delta(E_a - RT) / \sum n' = \left[v_0 + v_0 x_0 (n_x + n_y)\right] \quad (10)$$

Thus $E_0 \neq v_0$, i.e. E_0 does not correspond directly to the critical vibrational frequency but serves as an approximation. In the following treatment, for simplicity, we set $v_0 = v$ and estimate the anharmonicity using the data in Table 5 and Eq. 10,

$$v_0 x_0 = (680 - 720)/16 = -2.5\ \mathrm{cm}^{-1}. \quad (11)$$

The accuracy of E_0 depends on our choice of n' [see Eq. 3]. Taking one of the n' numbers to have a value higher or lower by one unit, i.e. $\sum n' = 26$ or 24, gives $E_{0+} = 7.82$ kJ mol^{-1} and $E_{0-} = 8.47$ kJ mol^{-1} where $E_0 = 8.13 \pm 0.35$ kJ mol^{-1}. Following the procedure adopted above, the vibrational quantum numbers were set to the integer value of $(E_a - RT)/E_{0+}$ and $(E_a - RT)/E_{0-}$ and the results are presented in Table 6. The variation of $E_a - RT$ with the calculated n values was fitted to a second order polynomial and the resultant fit (see Fig. 5a) can be represented by

$$E_a - RT = M_0 + M_1 n + M_2 n^2 \quad (12)$$

Table 6 Determination of vibrational quantum numbers where $E_0 = E_{0+} = 7.82$ kJ mol^{-1} (n_+) and $E_0 = E_{0-} = 8.47$ kJ mol^{-1} (n_-)

$(E_a - RT_{mean})$ (kJ mol^{-1})	$(E_a - RT_{mean})/7.82$	n_+	$(E_a - RT_{mean})/8.47$	n_-	n
48.27	6.18	6	5.70	6	6
42.38	5.42	5	5.00	5	5
82.42	10.55	11	9.73	10	10
66.04	8.45	8	7.80	8	8
70.14	8.98	9	8.28	8	9
62.30	7.97	8	7.36	7	8
51.23	6.56	7	6.05	6	6
108.70	13.90	14	12.83	13	13

The values for n are taken from Table 5

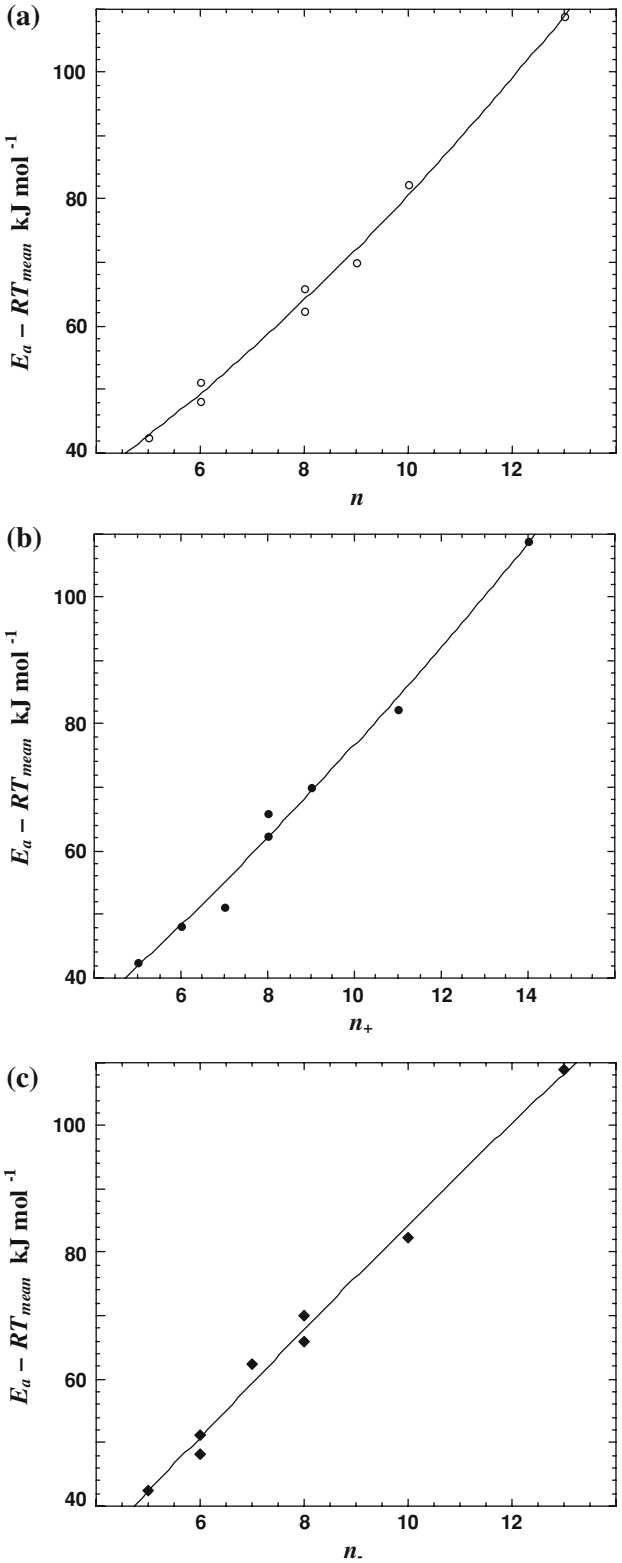

Fig. 5 Dependence of the (experimentally determined) $E_a - RT_{mean}$ on the (estimated) vibrational quantum number for three cases: **a** n: $E_a - RT_{mean} = 16.01 + 4.21n + 0.23n^2$; **b** n_+: $E_a - RT_{mean} = 11.85 + 5.49n_+ + 0.10n_+^2$; **c** n_-: $E_a - RT_{mean} = -2.51 + 9.23n_- - 0.06n_-^2$; correlation coefficient > 0.995

where $M_0 = 16.01$ kJ mol^{-1}, $M_1 = 4.21$ kJ mol^{-1} and $M_2 = 0.23$ kJ mol^{-1}. The positive value of the vibrational anharmonicity extracted from Eq. 12 is not consistent with theory. The use of the alternative higher and lower values of E_0 generates the vibrational quantum number values recorded in Table 6. The resulting second order polynomial fits for the variation of $E_a - RT$ with n_+ and n_- are given in Fig. 5b, c, respectively. A negative value for the second order term ($M_2 = -0.06$ kJ mol^{-1}) is obtained for n_-. The three points define a set of interpolation plots of M_0 versus M_1 and M_2 versus M_1 that are given in Fig. 6a, b. Taking the M_1 value that corresponds to the vibrational frequency (720 ± 29 cm^{-1}, i.e. $M_1 = 8.6 \pm 0.3$ kJ mol^{-1}) derived from the isokinetic temperature, these graphs can be used to estimate M_0 (0 ± 1 kJ mol^{-1}) and M_2 (-0.04 ± 0.01 kJ mol^{-1}). The latter corresponds to an anharmonicity

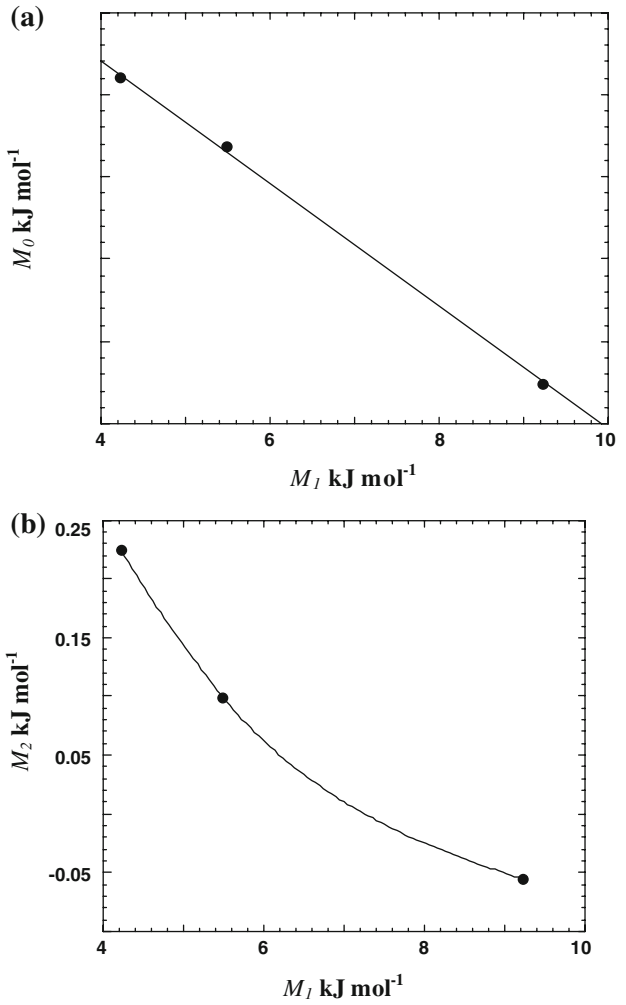

Fig. 6 Interpolation plots of **a** M_0 versus M_1 and **b** M_2 versus M_1 using the M_1 values associated with n, n_- and n_+. The values of M_0 and M_2 are obtained where $M_1 = 8.62$ kJ mol^{-1} corresponding to 720 cm^{-1}, i.e. the value of ν obtained from the calculation of T_{iso} (Table 4)

value of -3.3 ± 0.9 cm^{-1}, which is in good agreement with that (-2.5 cm^{-1}) obtained from Eq. 11 based on the approximation that $n_x + n_y = 16$. We can conclude that the experimental data indicate a critical vibration mode $(\nu) = 720 \pm 29$ cm^{-1} with an associated anharmonicity $(\nu_0 x_0) = -3.3 \pm 0.9$ cm^{-1}.

3.4 Mechanistic Considerations

The value for the critical vibrational mode extracted from our treatment of the experimentally hydrodeoxygenation kinetic data falls within the range of out-of-plane C–H vibrations that have been reported in the literature and which are compiled in Table 7. The tabulated values exhibit some variation depending on the nature of the substituent. Where two bands have been reported (in the case of *m*-disubstituted species) we have taken the wave number closest to the value(s) reported for the mono-substituted reactant [43]. It is significant that the value for the anharmonicity term that we have obtained is characteristic of bending vibrational modes [42]. Bending vibrations typically exhibit a lower anharmonicity parameter relative to (asymmetric) vibrations [44–46]. In terms of the SET model, our value of $\nu = 720 \pm 29$ cm^{-1} must be matched with a complementary vibrational mode in the catalyst system that supports resonance at this wave number, i.e. the catalyst donates resonance-energy to activate the C–H out-of-plane vibration. As the hydrogen mediated deoxygenation reactions were promoted using a Ni/SiO_2 catalyst, an obvious choice of vibrational mode is that corresponding to a Ni–H vibration. Indeed, Ni–H vibration modes have been measured using an inelastic neutron scattering (technique [47, 48]. In the case of Raney Ni–H systems [43], there are two sets of vibrations in the range of

Table 7 C–H out-of-plane vibrations (ν_{11}) obtained from the literature

Compound	ν_{11} cm^{-1}	Reference
Benzyl alcohol	738/748	[31]
m-methyl benzyl alcohol	737	[32]
Benzaldehyde	746	[33]
	740	[34]
	742	[35]
m-tolualdehyde	778	[36]
Benzoic acid	710	[37]
	708	[38]
	710	[39]
	710	[40]
m-toluic acid	745	[41]
o-Phthalic acid	742	[42]
Mean value (RMS)	743 ± 7	

interest to us. Firstly, there is one belonging to a threefold hollow site (C_{3v} symmetry) with an asymmetric stretch (E) at 940 cm^{-1} and a symmetric stretch (A_1) at 1,100 cm^{-1}. In addition, there is a second set of vibrations with a further modification of the C_{3v} symmetry, i.e. a broad band at 780 cm^{-1} related to the E term and a symmetric stretch (A_1) at 1,080 cm^{-1}. This change of the E symmetry has been treated in detail by Jobic and Renouprez [48] who have suggested that the 780 cm^{-1} band results from two modes at 750 and 815 cm^{-1} (± 10 cm^{-1}). They have proposed that the catalytic site associated with this interaction deviates from a perfect C_{3v} hollow, which is characterised by the band at 940 cm^{-1}. The mean of the out-of-plane vibrations for the seven reactants included in Table 7 is 743 ± 7 cm^{-1}. This variation is similar to the experimental uncertainty associated with our measure of the wave number for the critical vibration mode, i.e. 720 ± 29 cm^{-1} (or $T_{iso} = 518 \pm 21$ K). In our previous investigation [2], where only one reactant was considered, we obtained a T_{iso} value with a lesser associated uncertainty, i.e. ± 2 K. The larger error encountered in this study arises from the greater range of reactants considered. The agreement between the out-of-plane C–H vibrations ($\nu = 743 \pm 7$ cm^{-1}) for the aromatic alcohols, aldehydes and acids and the relevant Ni–H vibration with a distorted E symmetry ($\nu_{Ni-H} = 750 \pm 10$ cm^{-1}) represents the "perfect" resonance that is a requirement of the SET model.

Our analysis is then consistent with Ni–H vibrations serving as the source of catalytic energy, operating on a C–H out-of-plane vibration of the oxygenated arene. One consequence of the data treatment undertaken in this study is that the Q term in Eq. 4 approaches zero, suggesting that the reacting species are weakly held on the catalyst surface. In previous SET analyses of chlorobenzene hydrodechlorination [3] and benzene hydrogenation [49], it was established that the reactant is weakly adsorbed on the catalyst with a low associated heat of adsorption. We propose that it is necessary for the reacting molecule to loosely interact with the surface in order not to lose the (vibrational) energy excess to the phonons of the solid material. It must be stressed that we are considering a condensed phase reaction rather than a gas phase transformation where the associated kinetic theory is more simple. The molecule when excited extracts a hydrogen atom from Ni–H to fill the empty coordination position that is created by the out-of-plane movement of the C–H bond. This is faciltated by the excess number of sites on the surface where the reactant can adsorb. This situation stands in contrast to homogeneous catalysis (by metal complexes) where all reactants are coordinated (adsorbed) to one and the same metal atom (ion) and where, consequently, conversion is facilitated as the reactants are held in close proximity. It should also be noted that we have matched our catalytically significant vibration mode to reference values based on free molecule spectral data and any appreciable catalyst/reactant interaction(s) should result in some deviation of the vibrational frequencies relative to the free molecule. A consequence of the close agreement of the reference vibrational frequency with that obtained from experimentally determined activation energies is that the aromatic reactant is loosely bound to the catalyst.

4 Conclusions

The kinetics of the gas phase hydrodeoxygenation of a range of aromatic alcohols, aldehydes and acids (to the parent arene) have been measured over a common (1.5% w/w) Ni/SiO_2 catalyst. Compensation behaviour has been established with an associated isokinetic temperature (T_{iso}) $= 518 \pm 21$ K. The occurrence of this T_{iso} is accounted for in terms of the SET model where an aromatic vibrational mode (out-of-plane C–H vibration) is proposed that matches a complementary catalyst vibrational mode (Ni–H vibration) to support optimum resonance-energy transfer. The SET analysis has delivered a wavenumber of 720 ± 29 cm^{-1} as representing the critical resonance vibration with an associated anhamonicity term of -3.3 ± 0.9 cm^{-1}. This frequency agrees well with the reference out-of-plane vibrations for the aromatic reactants and a corresponding Ni–H vibration with a distorted E symmetry. A consequence of the agreement of the reference vibrational frequency for the substituted arenes that is obtained from free molecule spectral data with that inferred from our experimentally determined hydrodeoxygenation activation energies is that the reacting aromatic species are loosely bound to the catalyst surface.

References

1. Keane MA, Larsson R (2006) J Mol Catal A Chem 249:158
2. Keane MA, Larsson R (2007) J Mol Catal A Chem 268:87
3. Keane MA, Larsson R (2008) Catal Commun 9:333
4. Ho TC (1988) Catal Rev-Sci Eng 30:117
5. Furimsky E (2000) Appl Catal A Feneral 1999:147
6. Keane MA (2007) J Chem Technol Biotechnol 82:787
7. Luik H, Johannes I, Palu V, Luik L, Kruusement K (2007) J Anal Appl Pyrol 79:121
8. Moreau C, Joffre J, Saenz C, Geneste P (1990) J Catal 122:448
9. Moreau C, Aubert C, Durand R, Zmimita N, Geneste P (1988) Catal Today 4:117
10. Gates BC, Katzer JR, Schuit GCA (1979) Chemistry of catalytic processes. McGraw-Hill, New York
11. Kieboom APG, Van Rantwijk F (1977) Hydrogenation and hydrogenolysis in synthetic organic chemistry. Delft University Press, Delft

12. Augustine RL (1965) Catalytic hydrogenation. Marcel Dekker, New York
13. Absi-Halabi M, Stanislaus A, Trimm DL (1991) Appl Catal 72:193
14. Grange P, Vanhaeren X (1997) Catal Today 36:375
15. Furimsky E, Massoth FE (1999) Catal Today 52:381
16. Senol OI, Viljava TR, Krause AOI (2007) Appl Catal A Gen 326:236
17. Keane MA (1994) Can J Chem 72:372
18. Yuan G, Louis C, Delannoy L, Keane MA (2007) J Catal 247:256
19. Amorim C, Yuan G, Patterson PM, Keane MA (2005) J Catal 234:268
20. Welty JR, Wicks CE, Wilson RE (1984) Fundamentals of momentum, heat and mass transfer. Wiley, New York
21. Tavoularis G, Keane MA (1999) J Chem Technol Biotechnol 74:60
22. Burattin P, Che M, Louis C (1997) J Phys Chem B 101:7060
23. Coenen JWE (1991) Appl Catal 75:193
24. Burattin P, Che M, Louis C (1999) J Phys Chem B 103:6171
25. Bond GC, Keane MA, Kral H, Lercher JA (2000) Catal Rev Sci Eng 42:323
26. Linert W, Jameson RF (1989) Chem Soc Rev 18:477
27. Larsson R (1989) J Mol Catal 55:70
28. Larsson R (1987) Chem Scr 27:371
29. Bond GC (1985) Z Phys Chem 144:21
30. Larsson R (1989) Catal Today 4:235
31. Prystupa DA, Anderson A, Torrie BH (1994) J Raman Spectrosc 25:175
32. Integrated Spectral Database System of Organic Compounds (2008) National Institute of Advanced Industrial Science and Technology (AIST), Japan. http://riodb01.ibase.aist.go.jp/sdbs/. Accessed 14 Oct 2008
33. Zwarich R, Smolarek J, Goodman L (1971) J Mol Spectrosc 38:336
34. Green JHS, Harrison DJ (1976) Spectrochim Acta 32A:1265
35. Lampert H, Mikenda W, Karpfen A (1997) J Phys Chem A 101:2254
36. Etzkorn T, Klotz B, Sørensen S, Patroescu IV, Barnes I, Becker KH, Platt U (1999) Atmos Environ 33:525
37. Bakker JM, Aleese LM, von Helden G, Meijer G (2003) J Chem Phys 119:11180
38. Boczar M, Szczeponek K, Wojcik MJ, Paluszkiewicz C (2004) J Mol Struct 700:39
39. Antony J, von Heiden G, Meijer G, Schmidt B (2005) J Chem Phys 133:14305
40. Klausberger G, Furic K, Colombo L (1977) J Raman Spectrosc 6:278
41. Keller RJ (ed) (1986) The Sigma Library of FT-IR Spectra. Sigma Chemical Company Inc., Missouri
42. Colombo L, Volovsek V, LePostollec M (1984) J Raman Spectrosc 15:252
43. Bellamy LJ (1962) The infra-red spectra of complex molecules. Methuen & Co Ltd, London
44. Herzberg G (1962) Infrared and Raman spectra of polyatomic molecules. Van Nostrand, New York
45. Goodman L, Ozkebook AG, Thakar SN (1991) J Phys Chem 95:9044
46. Larsson R, Jamroz MH, Borowiak MA (1998) J Mol Catal A 129:41
47. Mitchell PCH, Parker SF, Ramirez-Cuesta AJ, Tomkinson J (2005) Vibrational spectroscopy with neutrons. World Scientific Publ. Co, Singapore
48. Jobic H, Renouprez A (1984) J Chem Soc Farady Trans I 80:1991
49. Bratlie KM, Li Y, Larsson R, Somorjai GA (2008) Catal Lett 121:173